Structural Analysis of the Voltage-Dependent Calcium Channel β Subunit Functional Core and Its Complex with the α1 Interaction Domain

Yarden Opatowsky,[1] Chien-Chang Chen,[2]
Kevin P. Campbell,[2,3] and Joel A. Hirsch[1,*]
[1]Department of Biochemistry
Faculty of Life Sciences
Tel Aviv University
Ramat Aviv 69978
Israel
[2]Department of Physiology and Biophysics
[3]Howard Hughes Medical Institute
University of Iowa
Iowa City, Iowa 52242

Summary

Voltage-dependent calcium channels (VDCC) are multiprotein assemblies that regulate the entry of extracellular calcium into electrically excitable cells and serve as signal transduction centers. The α1 subunit forms the membrane pore while the intracellular β subunit is responsible for trafficking of the channel to the plasma membrane and modulation of its electrophysiological properties. Crystallographic analyses of a β subunit functional core alone and in complex with a α1 interaction domain (AID) peptide, the primary binding site of β to the α1 subunit, reveal that β represents a novel member of the MAGUK protein family. The findings illustrate how the guanylate kinase fold has been fashioned into a protein-protein interaction module by alteration of one of its substrate sites. Combined results indicate that the AID peptide undergoes a helical transition in binding to β. We outline the mechanistic implications for understanding the β subunit's broad regulatory role of the VDCC, particularly via the AID.

Introduction

The passage of Ca^{2+} in a selective manner across the lipid bilayer of the cellular plasma membrane occurs by way of several protein families, one of them being voltage-dependent calcium channels. These channels are multiprotein assemblies that serve as "switchboards" for the highly regulated Ca^{2+} signal. They communicate with a large number of cellular players involved in amplifying, terminating, or modulating this critical pathway.

Two classes of assemblies gate the flow of Ca^{2+} in response to the voltage state of the plasma membrane. The structurally related but distinct classes are sensitive to low (Ca$_V$3) or higher (Ca$_V$1 or 2) relative voltage shifts (Jones, 1998). Ca$_V$1 or 2 subfamilies couple excitation of the cell to a variety of processes, depending on cell type, including contraction, secretion, and transcription. Furthermore, signal pathway crosstalk requires regulation of channel action by a small host of molecules. An example of such interactions is the GPCR signaling modulation of Ca$_V$2 channels (Dolphin, 2003b). Associa-

tion of liberated Gβγ with the calcium channel as a result of GPCR activation has a notable effect on function, with Gβγ behaving as an allosteric effector.

The VDCC (Ca$_V$1 or 2), as defined by biochemical purification of the stable complex, comprises four distinct polypeptides: α1, α2δ, β, and γ (Catterall, 1996). α1 is the membrane pore forming subunit, which contains four transmembrane domain repeats, paralleling the tetrameric architecture of potassium channels. Each domain contains the canonical voltage-dependent ion channel organization, i.e., six putative transmembrane segments. The membrane domains are connected by linkers located in the intracellular milieu, as are both the amino and carboxyl termini (Tanabe et al., 1987). β, in contrast, is a soluble and intracellular protein. Four separate β genes have been cataloged, each with multiple splice variants (Dolphin, 2003a). All four genes are expressed in the brain, while other tissues exhibit essential gene-specific expression, giving rise to embryonic lethality in β1 and β2 knockout mice (Ball et al., 2002). β3 and β4 knockouts or alleles lead to pathologies in a variety of physiological systems (Dolphin, 2003a).

Since molecular cloning of β, much attention has been focused on its role in VDCC function. Two major directions emerged from these studies. First, β facilitates the proper localization or trafficking of the VDCC and the α1 subunit in particular to the cellular plasma membrane (Herlitze et al., 2003). Several different β isoforms chaperone the channel to its target. Second, β acts as an important modulator of the channel's electrophysiological properties (Walker and De Waard, 1998). β alters activation and inactivation kinetics, causes a leftward shift in the I-V curve and, on the single channel level, induces an increase in the channel opening probability. Furthermore, the localization functionality has a marked impact on the electrophysiological aspect by increasing the number of channels at the membrane, significantly enhancing current amplitude (Chien et al., 1995).

The groundwork for understanding β's molecular mechanism was laid with the discovery by Campbell and coworkers that β bound α1 through a region in the linker between domains I and II (Pragnell et al., 1994), labeled the AID (for α1 interaction domain). Later studies have shown that β also interacts with other regions of α1 (Canti et al., 1999; Stephens et al., 2000; Tareilus et al., 1997; Walker et al., 1998, 1999), depending on the isoform, but the AID appears to be the primary, high-affinity site of interaction. Notably, structure-function research has implicated the AID itself in playing a critical role in channel activity, especially in terms of its effects on current inactivation parameters (Stotz et al., 2004).

Examination of β's structure and functional correlates has been more limited. Sequence analysis of the various genes from differing species supported a division of the protein into two central conserved motifs flanked by diverging sequences (De Waard et al., 1994). Biochemical and electrophysiological experiments showed that the second conserved motif was responsible for binding to the α1 subunit, and functional expression could recapitulate much of the full-length protein's functionality.

*Correspondence: jhirsch@post.tau.ac.il

Table 1. Data Statistics

| Data Collection and Phasing Statistics | SeMet β | | | | |
	λ_1	λ_2	λ_3	β	AID/β
Wavelength (Å)	0.97905	0.97854	0.90499	0.933	1.0069
Space group		P2₁2₁2		P2₁2₁2	P2₁2₁2
Unit cell parameters (Å)		a = 74.3		a = 74.1	a = 72.8
		b = 165.7		b = 163.8	b = 168.3
		c = 34.6		c = 34.8	c = 34.6
Total reflections	84,558	76,495	63,504	71,732	89,743
Unique reflections	9,990	9,969	8411	18,271	19,123
Completeness (%)[a]	98.8 (94.7)	98.6 (93.7)	95.4 (91.8)	92.8 (87.9)	85.7 (63.2)
R_{merge} (%)[a,b]	6.1 (21)	5.9 (19)	9.6 (21)	4.8 (31)	5.9 (31)
I/σ[a]	30.1 (9.7)	29.1 (9.7)	25.6 (10.5)	15.4 (4.3)	21.3 (3.9)
Resolution range (Å)	50–2.9	50–2.9	50–3.0	50–2.3	50–2.2
f'/f″	−9.68/2.30	−7.68/4.10	−1.33/3.14		
Phasing power (anomalous)	0.4	0.6	0.6		
Phasing power (dispersive)	0.5 (λ_2 vs λ_1)	0.7 (λ_3 vs λ_2)	0.9 (λ_1 vs λ_3)		
Figures of merit		0.39			
Beamline (ESRF)	BM-14	BM-14	BM-14	ID-14-2	ID-29

[a] Values for the highest resolution shell are given in parentheses.
[b] $R_{merge} = \Sigma_{hkl}\Sigma_i|I_{hkl,i} - <I>_{hkl}|/\Sigma_{hkl}\Sigma_i|I_{hkl,i}|$ where I_{hkl} is the intensity of a reflection and $<I>_{hkl}$ is the average of all observations of this reflection and its symmetry equivalents.

These two motifs were subsequently noted to be homologous to the SH3 and the guanylate kinase families, respectively (Chien et al., 1998; Hanlon et al., 1999). Recently, we showed experimentally that these two conserved motifs represent two bona fide folded domains with a removable intervening linker (Opatowsky et al., 2003). In addition, these domains interact in a stable fashion and represent a functional core of the full-length β protein. We now report a crystallographic analysis of the β functional core alone and in complex with an AID peptide. The results outline a conceptual framework for understanding β's function in the context of the VDCC and other possible roles.

Results and Discussion

Structure Determination
We determined the structure of the rabbit β2a functional core by performing a three-wavelength MAD experiment on a single crystal of selenomethionine-substituted protein (Tables 1 and 2). Experimental electron density maps at 2.9 Å resolution enabled tracing of the complete molecule with two clearly defined domains, as anticipated. Refinement of the atomic model continued with a 2.3 Å data set. Diffraction data to 3.5 Å was obtained for an alternate crystal form, crystallized with two different forms of the functional core protein. A molecular replacement solution and refinement indicated no significant conformational differences between this and its higher resolution form. Thus, our analysis focuses on the high-resolution form. Subsequently, we cocrystallized the β functional core with an 18 residue peptide, whose sequence is derived from the Ca$_V$1.1 AID. This crystal form unequivocally contained the AID peptide, as we could also cocrystallize β with a fluorescein-labeled peptide that gave bright yellow crystals. Diffraction data on the cocrystal was measured to a d$_{min}$ of 2.2 Å, and the AID/β complex structure was determined by molecular replacement and rounds of model building and refinement. The initial electron density for the bound AID peptide is shown in Figure 4A. Residues 25–33 (N terminus), 203–217 (truncated linker), and 416–422 (C terminus) of β are not visible in the electron density maps.
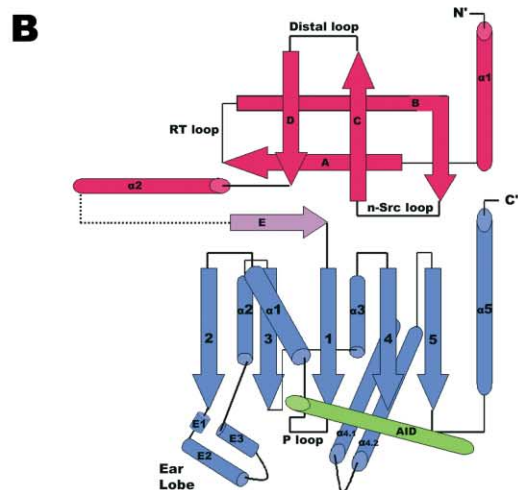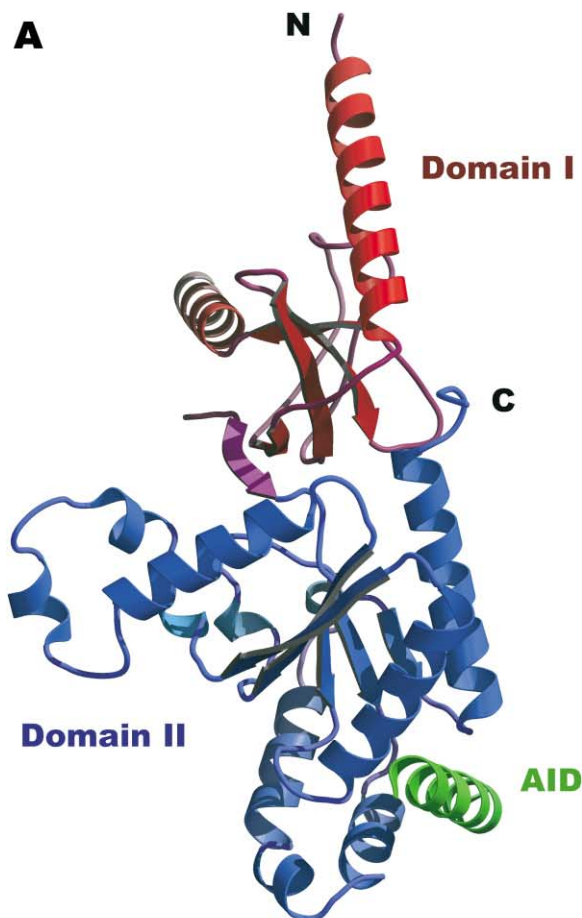
Molecular Architecture
The structure reveals a two-domain construction (Figure 1A) with dimensions 94 × 54 × 48 Å and defines a new variant of the membrane-associated guanylate kinase (MAGUK) protein family (Dimitratos et al., 1999). MAGUK proteins have been defined generally by sequences that contain three modules, namely PDZ, SH3, and guanylate kinase-like (Guk) domains. Many of the members contain multiples of the PDZ domain. Family members function as molecular scaffolds, using their various domains to create a web of protein-protein interactions at or near the cell membrane. VDCC β lacks the PDZ domain, but its domain I is most similar to MAGUK SH3 domains, while its domain II is a GuK-like domain. In certain respects, β represents a minimal MAGUK, having eliminated the PDZ domain and dressed down its GuK domain as detailed below. The structure of the SH3 and GuK domains from a MAGUK protein, PSD-95, serves as a critical foil for our structural analysis (McGee et al., 2001; Tavares et al., 2001).

The structure of domain I is best described as an

Table 2. Refinement Statistics

Refinement Statistics	β	AID/β
No. of reflections (working/test)	17,294/935	17,364/1,283
d$_{min}$ (Å)	2.3	2.2
R$_{work}$/R$_{free}$	26.1/28.8	23.3/28.8
Rms deviation from ideality		
Bond lengths (Å)	0.013	0.011
Bond angles	1.3°	1.3°
B factors (Å²) (rmsd of bonded atoms-main/side chain)	1.1/2.1	1.0/2.1
Average B factor (Å²)	62.7	44.1
No. of protein atoms/solvent	2299/91	2541/130

A

N

Domain I

C

Domain II

AID

B

adorned SH3 domain. The fold is shown schematically in Figure 1B. Long α helices are appended to the module's amino terminus and as an insertion between the fourth and fifth strands. Strand E belongs formally to the SH3 architecture while it is nominally part of domain II, since limited proteolysis removes the polypeptide connecting helix 2 to strand E, leaving it with the latter domain. Helix 1, not seen in PSD-95, is found in the β structure to partially unwind toward the visible end of its N terminus. Helix 2 is present in PSD-95 but with a somewhat different orientation. The rms deviation after superposition between domain I and the Crk SH3 domain (Wu et al., 1995) is 1.3 Å for 52 Cα atoms, while the rmsd between domain I and the SH3 of PSD is 1.3 Å for 61 Cα atoms.
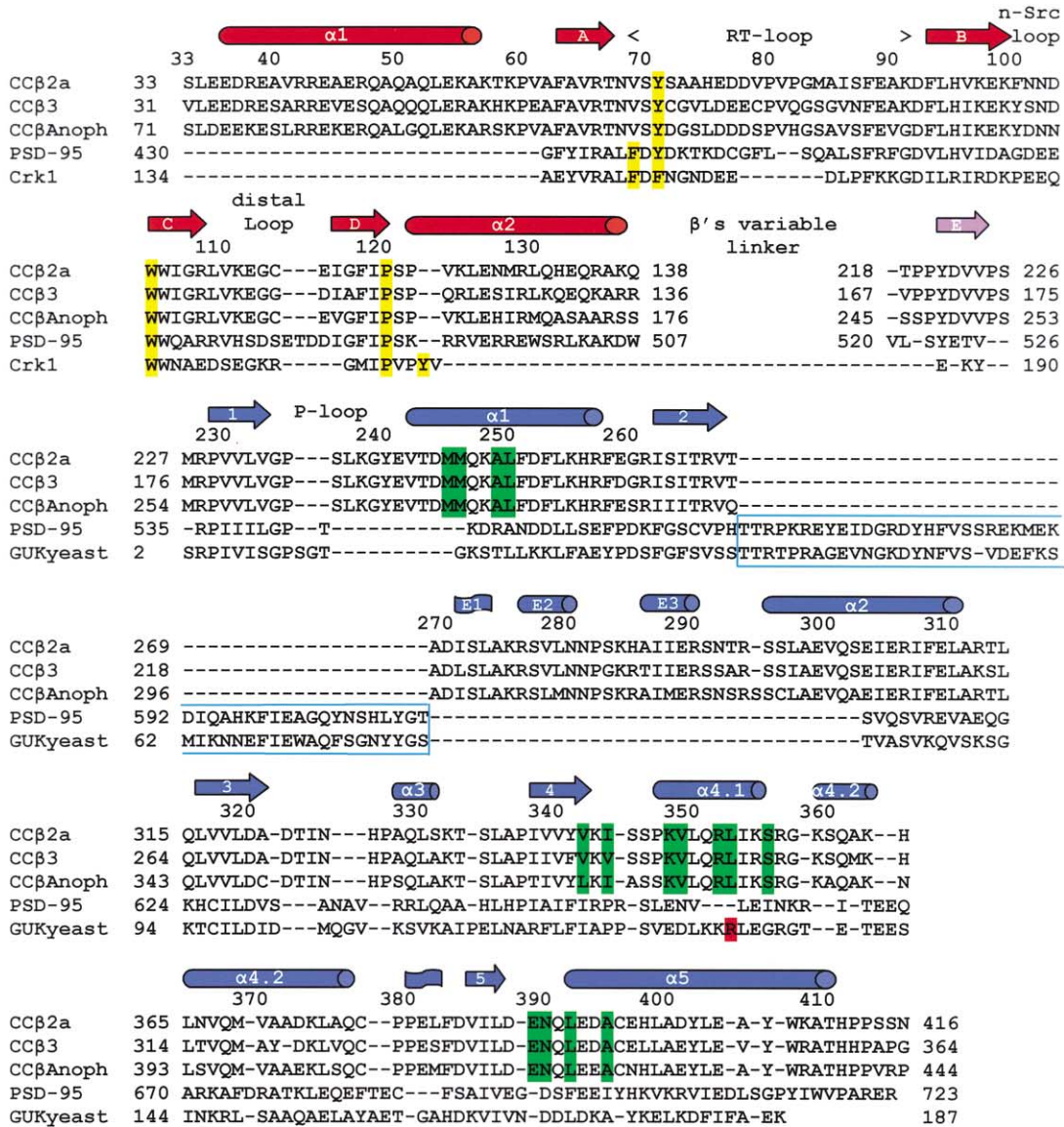
A significant difference between domain I and the SH3 fold lies in β's unusually long extended RT loop. Using its length, as seen in Figure 3A, the β RT loop takes a different conformation than that of PSD-95, folding in toward the n-Src loop and interacting with W104, thereby occluding the canonical polyproline binding groove. Both helices 1 and 2 make important interactions with parts of the SH3 fold. Helix 1 (E46, A49, L53) contains hydrophobic interactions with the RT loop (residues 80–84) and strands A, B, C, and D so that it is well integrated into the fold. At the same time, helix 2 interacts with the hydrophobic core of the domain through interactions from its side chains L125 and M128. Thus, helix 2 projects outward from the SH3 fold precisely where the polyproline lies in its groove on the superposed Crk SH3 domain. Moreover, L125 anchors the helix at about the same position of conserved hydrophobic residues in polyproline ligands, i.e., the amino terminus of helix 2 uses similar structural determinants to anchor itself to the domain as do canonical SH3 ligands.

Domain II has strong structural homology to GuK and the GuK-like domains found in MAGUKs (Figure 3B), and in general, to the P loop kinase superfamily (Leipe et al., 2003). The GuK fold has three subdomains: the core, comprised of a parallel five-stranded β sheet sandwiched by five helices, the mononucleotide binding (NMP) subdomain, and the helical lid subdomain. VDCC β contains both the core and lid subdomains but substitutes the NMP subdomain with a structurally unrelated subdomain of about the same length, comprising several short helices, which we have called the "ear" lobe (Figure 1B). In contrast, the MAGUKs retained the NMP subdomain, comprising a three-stranded sheet and two helices including the ability to bind mononucleotides, in some cases. The rmsd between domain II and yeast GuK (Stehle and Schulz, 1992) is 1.6 Å for 128 Cα atoms and between PSD-95 GuK is 2.2 Å for 86 Cα atoms. These superpositions underline the stronger resem-

Figure 1. Structure of VDCC β Functional Core in Complex with the AID

Ribbon (A) and topology (B) diagrams of the VDCC β subunit functional core bound to the AID peptide. Domain I, domain II, and the AID are represented in red, blue, and green, respectively. The topology scheme for each domain was patterned and labeled after the relevant canonical motif.

A

```
                                                                                        n-Src
            α1                          A      <        RT-loop           >    B    loop
      33        40        50        60        70        80        90        100
CCβ2a     33  SLEEDREAVRREAERQAQAQLEKAKTKPVAFAVRTNVSYSAAHEDDVPVPGMAISFEAKDFLHVKEKFNND
CCβ3      31  VLEEDRESARREVESQAQAQLEKAHKPEAFAVRTNVSYCGVLDEECPVQGSGVNFEAKDFLHIKEKYSND
CCβAnoph  71  SLDEEKESLRREKERQALGQLEKARSKPVAFAVRTNVSYDGSLDDDSPVHGSAVSFEVGDFLHIKEKYDNN
PSD-95   430  -------------------------GFYIRALFDYDKTKDCGFL--SQALSFRFGDVLHVIDAGDEE
Crk1     134  -------------------------AEYVRALFDFNGNDEE-------DLPFKKGDILRIRDKPEEQ

               distal
            C   Loop      D           α2              β's variable
      110            120         130                 linker                E
CCβ2a     WWIGRLVKEGC---EIGFIPSP--VKLENMRLQHEQRAKQ 138       218 -TPPYDVVPS 226
CCβ3      WWIGRLVKEGG---DIAFIPSP--QRLESIRLKQEQKARR 136       167 -VPPYDVVPS 175
CCβAnoph  WWIGRLVKEGC---EVGFIPSP--VKLEHIRMQASAARSS 176       245 -SSPYDVVPS 253
PSD-95    WWQARRVHSDSETDDIGFIPSK--RRVERREWSRLKAKDW 507       520 VL-SYETV-- 526
Crk1      WWNAEDSEGKR-----GMIPVPYV------------------------------E-KY-- 190

             1      P-loop         α1             2
          230            240         250         260
CCβ2a    227  MRPVVLVGP---SLKGYEVTDMMQKALFDFLKHRFEGRISITRVT-------------------------
CCβ3     176  MRPVVLVGP---SLKGYEVTDMMQKALFDFLKHRFDGRISITRVT-------------------------
CCβAnoph 254  MRPVVLVGP---SLKGYEVTDMMQKALFDFLKHRFESRIIITRVQ-------------------------
PSD-95   535  -RPIIILGP--T-----------KDRANDDLLSEFPDKFGSCVPHTTRPKREYEIDGRDYHFVSSREKMEK
GUKyeast   2  SRPIVISGPSGT---------GKSTLLKKLFAEYPDSFGFSVSSTTRTPRAGEVNGKDYNFVS-VDEFKS

              E1    E2     E3            α2
           270    280     290       300        310
CCβ2a    269  --------------------ADISLAKRSVLNNPSKHAIIERSNTR-SSLAEVQSEIERIFELARTL
CCβ3     218  --------------------ADLSLAKRSVLNNPGKRTIIERSSAR-SSIAEVQSEIERIFELAKSL
CCβAnoph 296  --------------------ADISLAKRSLMNNPSKRAIMERSNSRSSCLAEVQAEIERIFELARTL
PSD-95   592  DIQAHKFIEAGQYNSHLYGT-----------------------------------SVQSVREVAEQG
GUKyeast  62  MIKNNEFIEWAQFSGNYYGS-----------------------------------TVASVKQVSKSG

             3        α3         4       α4.1    α4.2
          320       330        340      350       360
CCβ2a    315  QLVVLDA-DTIN---HPAQLSKT-SLAPIVVYVKI-SSPKVLQRLIKSRG-KSQAK--H
CCβ3     264  QLVVLDA-DTIN---HPAQLAKT-SLAPIIVFVKV-SSPKVLQRLIRSRG-KSQMK--H
CCβAnoph 343  QLVVLDC-DTIN---HPSQLAKT-SLAPTIVYLKI-ASSKVLQRLIKSRG-KAQAK--N
PSD-95   624  KHCILDVS---ANAV--RRLQAA-HLHPIAIFIRPR-SLENV---LEINKR--I-TEEQ
GUKyeast  94  KTCILDID---MQGV--KSVKAIPELNARFLFIAPP-SVEDLKKRLEGRGT--E-TEES

            α4.2                  5          α5
          370       380       390        400        410
CCβ2a    365  LNVQM-VAADKLAQC--PPELFDVILD-ENQLEDACEHLADYLE-A-Y-WKATHPPSSN 416
CCβ3     314  LTVQM-AY-DKLVQC--PPESFDVILD-ENQLEDACELLAEYLE-V-Y-WRATHHPAPG 364
CCβAnoph 393  LSVQM-VAAEKLSQC--PPEMFDVILD-ENQLEEACNHLAEYLE-A-Y-WRATHPPVRP 444
PSD-95   670  ARKAFDRATKLEQEFTEC---FSAIVEG-DSFEEIYHKVKRVIEDLSGPYIWVPARER 723
GUKyeast 144  INKRL-SAAQAELAYAET-GAHDKVIVN-DDLDKA-YKELKDFIFA-EK       187
```

B

```
                                    AID
Cav1.1 HUMAN 335  GEFTKEREKAKSRGTFQKLREKQQLDEDLRGYMSWITQGE
Cav1.2 HUMAN 406  GEFSKEREKAKARGDFQKLREKQQLEEDLKGYLDWITQAE
Cav1.3 HUMAN 407  GEFSKEREKAKARGDFQKLREKQQLEEDLKGYLDWITQAE
Cav1.4 HUMAN 373  GEFSKEREKAKARGDFQKRREKQQMEEDLRGYLDWITQAE
Cav2.1 HUMAN 361  GEFAKERERVENRRAFLKLRRQQQIERELNGYMEWISKAE
Cav2.3 HUMAN 353  GEFAKERERVENRRAFMKLRRQQQIERELNGYRAWIDKAE
Cav2.1 ANOPH 264  GEFAREREKVENRQEFLKLRRQQQLEKELNGFVEWICKAE
Cav2.2 ANOPH 316  GEFAREREKVENRQEFLKLRRQQQLEKELNGYVEWICKAE
Cav1.1 DISOC 349  GEFAKERERVENRRAFLKLRRQQQVEQEFNRYLRWIHIAE
Cav2.1 C.ELE 369  GEFSKEREKARARGLFQKFREKQQLEEDLKGYLDWITQAE
```

Figure 2. Sequence Alignment and Structural Features of VDCC β and the α1 I-II Linker

(A) Sequence alignment and secondary structure of the VDCC β functional core. Sequence of rabbit CCβ2a (GenBank accession number CAA45575.1), human CCβ3 (NP_000716.1), and *Anopheles gambiae* CCβAnoph (EAA12209.1) were aligned using CLUSTALW. For comparison, structure-based sequence alignment was performed with mouse c-Crk, N-terminal SH3 domain (Q64010, PDB-1CKA), *S. cerevisiae* guanylate kinase GUKyeast (KIBYGU, PDB-1GKY), and rat PSD-95 (NP_062567, PDB-1JXO). Secondary structure elements were assigned with DSSPcont (Andersen et al., 2002), with nomenclature and color codes as in Figure 1B. Arrows, cylinders, and flags denote β strands, α helices, and 3₁₀ helices, respectively. Highlighted in yellow are the residues involved in polyproline recognition in canonical SH3 domains, represented by Crk. Residues highlighted in green participate in AID/β interactions. Boxed in cyan is the NMP binding motif of guanylate kinase, as seen for yeast GUK and PSD-95. Arg131 of yeast GUK, essential for ATP binding, is highlighted in red.

(B) Alignment of the α1 subunit I-II linker until the end of the AID sequence. Accession numbers are as follows: HUMAN Cav1.1 (Q13698), Cav1.2 (Q13936), Cav1.3 (Q01668), Cav1.4 (O60840), Cav2.1 (O00555), Cav2.3 (Q15878), Cav2.1 ANOPH (EAA07643.1), Cav2.2 (EAA07643.1), Cav1.1 DISOC *Disc. ommata* (P56698), and Cav2.1 C.ELE *C. elegans* (AAB03158.4).

blance of β domain II in the two relevant subdomains to yGuK versus PSD-95.

Since β lacks the NMP subdomain, it is not expected to bind GMP, but it remains possible that the ear lobe will bind a small molecule since it does create clefts between itself and the central sheet and itself and strand 5 of domain I. Another important difference between β and GuK or PSD-95 is the P loop, also known as the Walker A box, which connects strand 1 and helix 1. As seen in Figures 2A and 3B, β's P loop is significantly longer than PSD and GuK. P loops in the kinase family are important for the binding of ATP phosphate moieties used for phosphotransfer. The composition and conformation of β's loop is pivotal for binding its target as described below. The lid subdomain is retained in all three structures in different orientations. β's lid orientation most closely approximates that of apoGuK (open) versus that of GuK with ADP bound (closed) (Sekulic et al., 2002) and PSD-95 (very closed). The difference in orientation may have important consequences for protein target binding. Finally, ATP will likely not bind β, as β lacks an essential arginine, R131 in yGuK, required for nucleotide binding in all guanylate kinases. In β, the arginine has been replaced with a leucine. This crucial structural difference between GuK and β predicts that phosphotransferase activity has been lost by β and most probably the whole MAGUK family.

How do the two domains interact and how does that organization compare to PSD-95? Strand E of domain I is covalently linked by a short four residue turn to domain II. In addition, other interactions include hydrogen bonds from domain II helix 5 made with the distal loop of domain I. Side chains from the ear lobe and a turn before strand 4 of domain II interact with strand E of domain I. While the individual domains and topology are similar to PSD-95, the actual 3D picture is quite different. Due to PSD-95's very long strand E, the nature of the domain apposition varies. PSD-95's strand F couples with strand E but is derived from the PSD-95 GuK domain. This is absent in β. The drastically different domain orientation is visualized in Figure 3C, where we have superposed the GuK-like domains. In addition, the domain interface in β is more intimate, burying more accessible surface area (1500 Å² versus 1200 Å²) than for PSD-95.

Protein-Protein Interaction Paradigm for GuKs

The GuK domain of the MAGUK family acts as a novel protein-protein interaction domain. Its function is required since several mutant phenotypic alleles of the founding member of the family, *Drosophila Discs large (dlg)*, encode truncated proteins that have their GuK domain deleted (Budnik et al., 1996). Subsequently, several instances of GuK domains from MAGUK proteins have been shown to bind to various protein targets (Hanada et al., 2000; Kim et al., 1997; Mathew et al., 2002; Takeuchi et al., 1997). Some of the target proteins are motor proteins, used for transporting cargoes to various cellular locations. However, it is unknown how the GuK domains bind these targets.

The AID peptide is found bound to β domain II, consistent with earlier studies that had defined a region of interaction with the AID. The AID forms an α helix that

nestles into a groove on the protein, shaped by the juxtaposition of the lid subdomain and the core subdomain P loop, helix 1, strand 5, and helix 5. Thus, the AID binds in the same location as does ATP in GuK, visualized in Figure 3B. Perhaps even more striking is the superposition of the adenosine moiety from ATP or ADP and the W369 of the AID. While the helical cylinder fits into the groove, the AID has two legs stapling it down. One leg consists of W369 and I370. W369 binds in a deep pit on the domain II surface and makes many interactions with domain II residues (summarized in Figure 4B). The stereochemistry of W369 is crucial. Most importantly, its Nε1 makes a hydrogen bond to the main chain carbonyl of M246 on β. Consequently, we can easily justify its absolute conservation (Figure 2B). The second leg consists of G365 and Y366. Y366 is buried completely, making van der Waals interactions with β. Concomitantly, its hydroxyl group makes bifurcated hydrogen bonds to two water molecules. These, in turn, mediate hydrogen bonds to β main chain carbonyl (389) or amine (345) groups. These residues are absolutely conserved except in the AID of the electric ray where the glycine is replaced with an arginine. The balance of connections involve van der Waals or hydrophobic interactions. Importantly, interactions between AID and domain II are not localized to one region in sequence space of β, so that earlier definitions of the β interacting domain (BID), residues 218 to 250 (i.e., strand E of domain I and strand 1, P loop, and half of helix 1 of domain II), are misleading. Three regions in sequence space contribute to the AID binding site, so that for proper binding of the AID, one requires almost the complete domain II.

Complexation of the AID with β results in the burial of 1640 Å² of accessible surface area. The average value for buried surface area among protein-protein interaction interfaces is around 1600 Å². However, the nature of the interface is somewhat unusual. Janin and coworkers, in a survey of protein-protein interaction interfaces, arrived at average number of hydrogen bonds and the amino acid propensity in these interfaces (Lo Conte et al., 1999). They find that these interfaces are more polar and involve more hydrogen bonds and ion pairs than protein interiors. In this way, the AID/β interface more resembles a protein interior. There is a paucity of hydrogen bonds (four, two being solvent mediated, versus an average of ten) and one probable ion pair, and almost all of the remaining interactions are van der Waals or hydrophobic interactions. The β residues in the interface are almost entirely nonpolar, while we do not detect a large number of solvent molecules in the interface.

The binding of β to mutagenized AID sequences has been investigated extensively in earlier work. Results of these studies are summarized in Figure 4C and complement our structural data. They underline the exquisite specificity of W369 and the importance of Y366 and I370. Perturbation of these residues essentially abrogates binding. In general, the importance of residues for binding correlates well with their relative burial upon association as computed from the crystal structure. Interestingly, mutation of Gly365 to arginine does not negate binding, suggesting that β will accommodate a bulkier side chain. The sequence conservation of glycine and its stereochemistry may be explained though the
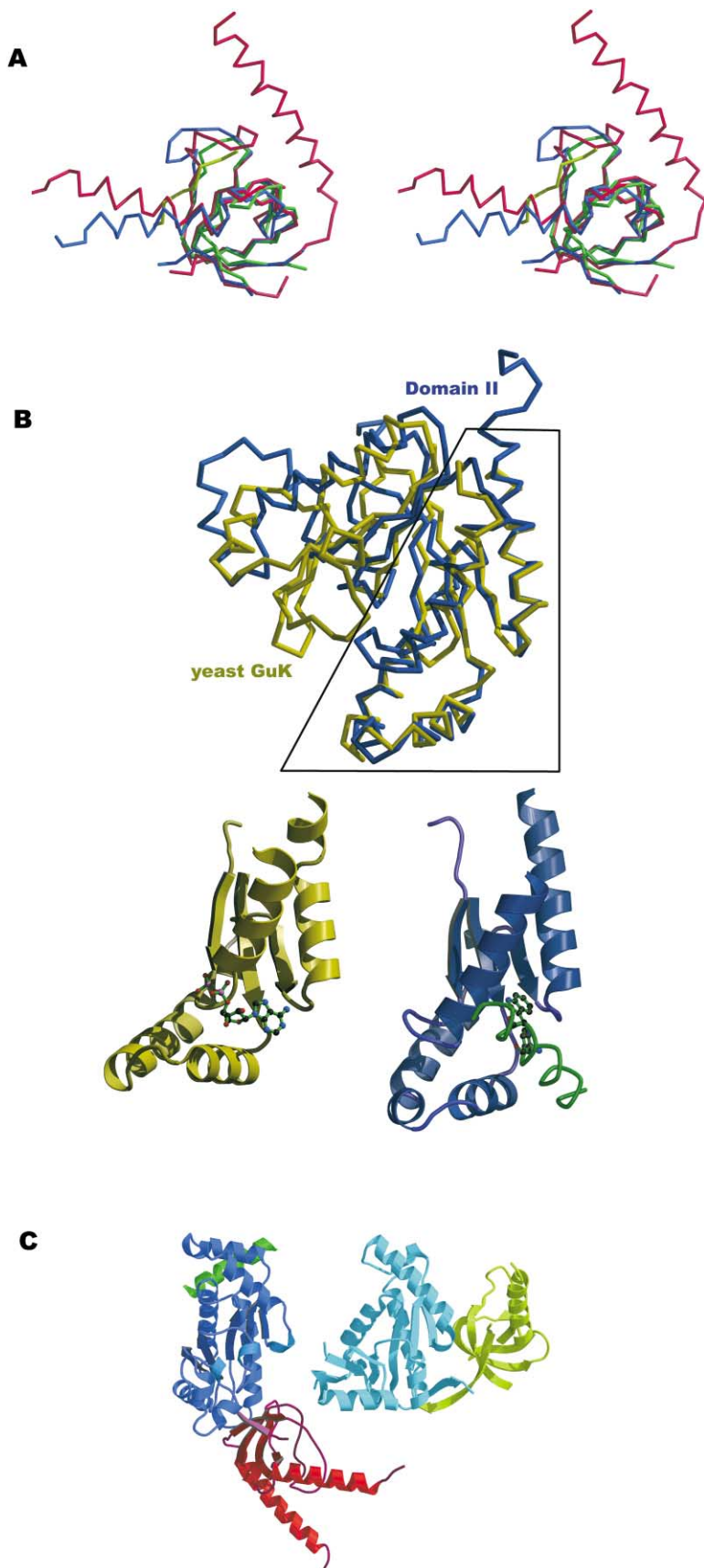
Figure 3. Superposition of VDCC β Functional Core with c-Crk SH3 Domain, GuK, and PSD-95

(A) Stereo diagram of β domain I (red), superimposed with PSD-95 SH3 domain (1JXO) (blue) and c-Crk SH3 domain (1CKA) (green) with a bound proline-rich peptide (yellow).

(B) β domain II (blue) superimposed with GuK (yellow). β domain II was superimposed with yeast Guk (1GKY) (top). The same perspective was used to compare the lid and core subdomains of the GuK fold from the AID-β complex and mouse GuK with bound ADP (1LVG) (bottom).

(C) AID bound β (left) and PSD-95 (right) after superposition of β domain II and the PSD GuK domain. PSD was then translated horizontally. β domain I, domain II, and AID are red, blue, and green, respectively, while the PSD SH3 and GuK domains are cyan and yellow, respectively.

dynamics of complexation, described below. Changes in other residues, particularly those of the AID's solvent-exposed helical face, have little effect on binding.

Mutagenesis of the β subunit and examination of the effects on AID association is less extensive. The BID had several residues mutated (De Waard et al., 1994). Those that had no effect on binding may be rationalized via the structure since they are far from the binding site. Two prolines that were changed to arginines but are distal from the binding site and affected binding should disrupt the protein folding since they are buried. We have characterized two new mutations of β that were designed based on the structure, M246 and L392. M246 is found toward the C-terminal end of the BID and L392 in the N-terminal end of helix 5. Both residues were changed to alanine, and binding constants to AID peptide were measured by fluorescence polarization. Both mutants lowered the affinity by one to two orders of magnitude (wt, $K_D = 26 \pm 6$ nM; M246, 1.7 ± 0.3 μM; L392, 0.34 ± 0.04 μM). These results corroborate our structural data that show the binding site to be composed of sequences outside of the BID.

A comprehensive search of the PDB, using FlexProt (Shatsky et al., 2002), for complexes that showed similarity to the AID/β interface led us to one hit. The crystal structure of the plasmid maintenance system from *Strept. pyogenes* constitutes a complex of the ζ toxin bound to its antitoxin ε (Meinhart et al., 2003). While the rmsd is 1.8 Å for 82 out of 183 Cα atoms with a 4% sequence identity, the mode of interaction and even the general architecture of the toxin is quite similar to β's domain II. The toxin has a P loop kinase fold and generated the proposal that it acts as a phosphotransferase. Mutation of residues putatively required for enzymatic activity abrogated toxicity, suggesting that the catalytic function is responsible for its killing potential. The antitoxin apparently acts by binding the toxin with its first helix inserting into the groove between the toxin's lid and core subdomains. Aromatics bury themselves into positions overlapping, in superpositions, that of W369 and the adenosine base of ATP/ADP of the GuKs.

The comparative structural analysis of the GuK fold lead us to the conclusion that this widely extant protein fold, found in every type of organism, evolved from an enzyme with phosphotransferase capacity to a protein-protein interaction module, losing on its way catalytic activity. Moreover, its ligand binding site was resculptured to enable protein-protein interactions. Striking examples of this resculpturing are the change of the absolutely required arginine (in yGuK, Arg131) into a leucine in β and the protein target using aromatic side chains in the place of the nucleotide base. In the case of ζ toxin, catalytic activity is retained and the protein-protein interface facilitates inhibition, while in the case of VDCC β, catalytic activity probably has been lost to an interface that obtains high affinity and stable binding for its protein target. We propose that the MAGUK family uses the same strategy for binding its protein targets through its GuK domain.

VDCC Assembly

Our results have important implications for understanding VDCC functional aspects. One aspect, its mecha-

nism for chaperoning the channel, has been elaborated by De Waard and coworkers (Bichet et al., 2000a; Cornet et al., 2002). They have shown that the α1 I-II linker contains an endoplasmic retention signal. β then successfully competes with an unknown ER retention protein in binding the linker via the AID, thereby masking the retention signal. This frees the channel to exit the ER and move ultimately to the plasma membrane with β still attached.
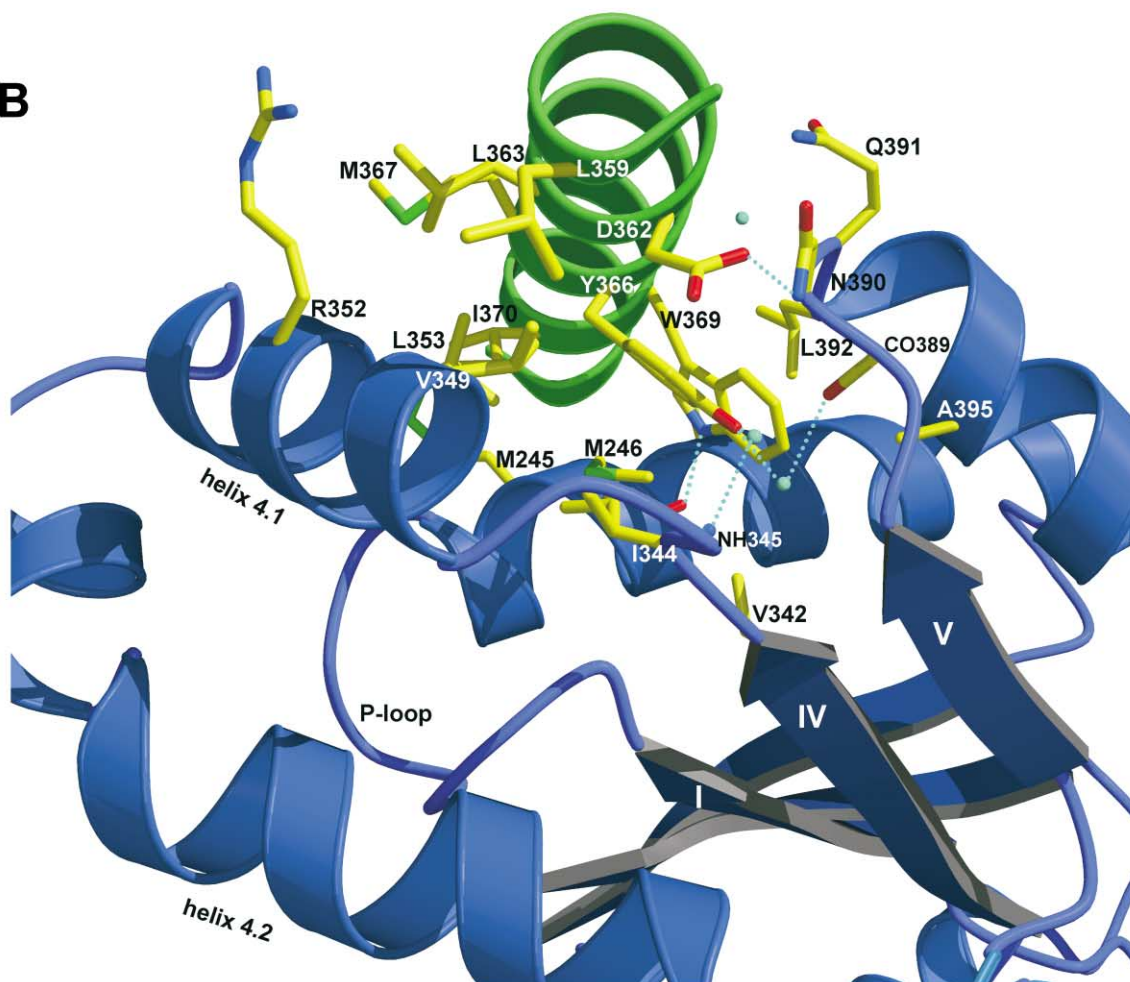
Given the crystallographic data that the AID is in an α-helical conformation in the complex, we asked what is its secondary structure when alone in solution? To address this question, we measured a circular dichroism (CD) spectrum of the peptide. The spectrum, shown in Figure 5, indicates a random coil structure. This implies that, at least in our in vitro system, the AID peptide undergoes a coil to helix transition during its association with β. We then measured the helical propensity of the AID peptide by taking a CD spectrum with the peptide in a mixed water/trifluoroethanol solution. The spectrum shows significant helical formation. Based on these data, it seems reasonable to posit that the AID associates with β in a coil conformation and undergoes a helical transition upon reaching its high-affinity bound state. This hypothesis is consistent with several observations. First, the nature of the protein-protein interface is largely nonpolar and provides the ideal environment for a folding surface, akin to the lower dielectric characteristic of the mixed water/trifluoroethanol solvent in the CD measurements. Such an environment is markedly more favorable energetically for the peptide backbone to make its hydrogen bonds than when faced with an aqueous environment (Luo and Baldwin, 1997; Yang and Honig, 1995). Second, the binding kinetics measured for the AID with β ($k_{on} \sim 2$–6×10^5 M^{-1}•s^{-1}; $k_{off} \sim 5 \times 10^{-3}$ s^{-1}) (Canti et al., 2001; Geib et al., 2002) suggest that the association is not a diffusion-controlled rigid body fast reaction ($k_{on} \sim 10^7$ M^{-1}•s^{-1}) (Schreiber, 2002). The values are consistent with a folding step wherein the AID encounters β, low-affinity binding occurs, and then the AID folds into its helix conformation, locking in the high-affinity binding mode with its myriad interactions. Binding reversibility was established both in vitro and in situ as assessed by electrophysiological assays (Restituito et al., 2001). In this vein, reversibility could be prevented in an AID mutant replacing the glycine with arginine (Bichet et al., 2000b). Given our conclusion that the AID folds onto β, we argue that the conserved glycine provides the reversibility by its low helical propensity (Pace and Scholtz, 1998). Third, an established method for detecting AID/β binding uses overlay assays wherein a fusion protein bearing the AID sequence is electrophoresed in a SDS system and transferred to nitrocellulose, and labeled β protein is used to probe the filter (Marquart, 1997; Pragnell et al., 1994). Despite the denaturing manner by which the AID is treated, β succeeds in binding avidly, suggesting that it can associate while the AID is initially unfolded.

We therefore propose that β acts not merely as chaperone, accompanying α1 through the trafficking/processing pathway, but also as a chaperonin for the I-II linker section of the channel. Such activity may be pivotal in insuring the fidelity of channel assembly. Moreover, we suggest that the helix induction does not occur

A

B

C

Figure 4. AID/β Interactions

(A) 2Fo − Fc electron density map, contoured at 1σ, of the AID, calculated following molecular replacement using the β model and the AID/β complex data set. The AID (green) is represented as bonds and the β is represented in blue ribbons.
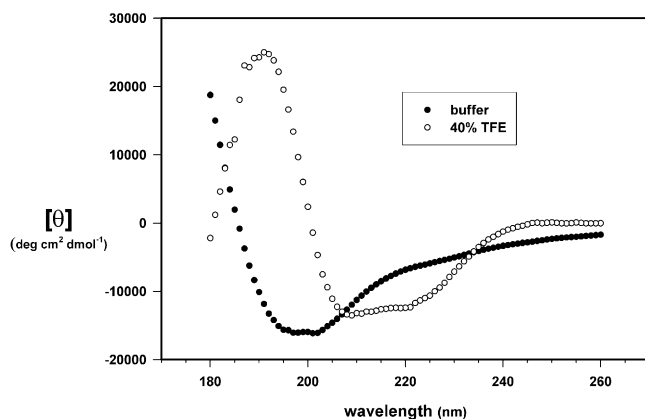
Figure 5. CD Spectroscopy of the AID Peptide in Solution

Spectra were measured in 2.5 mM Na phosphate (pH 8), 15 mM NaCl (filled circles) at a peptide concentration of 46 μM at 20°C and in 40% (vol/vol) trifluorethanol plus the above buffer (open circles). Deconvolution analysis (Bohm et al., 1992) indicates 9% helicity in buffer alone versus about 34% in the TFE solution.

just in the AID site. Importantly, the protein sequence of the I-II linker, starting from the C-terminal end of membrane domain I (i.e., the end of its S6 through the AID sequence motif), is predicted to be one long α helix by all secondary structure algorithms that we have tested. We thus extrapolate that β association with the I-II linker induces helix formation of the AID that is then propagated toward the S6 helix along the polypeptide sequence of the I-II linker.

Channel Structure and Function

Several groups have recently made progress toward elucidating the physical organization of VDCCs, using electron microscopy (Murata et al., 2001; Serysheva et al., 2002; Wang et al., 2003; Wolf et al., 2003). A monomeric complex has area dimensions of 110–150 × 120–165 Å. Identification of the extracellular α2δ has been made, along with a localization of β. The dimensions of the β functional core would fit well into the density. The β subunit, considering its elongated shape, comprises a significant fraction of the intracellular mass of the channel. This observation may be visualized in Figure 6A, where a schematic α1 subunit has been drawn to estimated scale with β bound to the α1 I-II linker that contains the AID.

Voltage-dependent channels feature two salient molecular characteristics: (1) they are highly ion selective, and (2) they enable permeation of these ions in reaction to the membrane electrical potential. Gating is controlled by the interaction between the voltage sensor (S1-4) subdomain and the helical pore subdomain (S5-6). The conformation of the pore in closed (Kcsa) and open (MthK) positions is known for K^+ channels (Jiang et al., 2002b). In order to transition between these two conformational states, it appears that S5 moves, induced by the voltage sensor, which in turn creates lateral torque on S6, causing its helix to bend near a glycine and move out radially, opening the channel. Using this information as a structural template, the S6 of the α1 membrane domain I is followed immediately by the I-II linker. The I-II linker starts with an absolutely conserved sequence (GEF), with the AID positioned exactly 22 residues later in all cases and whose intervening sequences are highly conserved (Figure 2B). This structure is bound in a noncovalent but stable manner to β. We infer that VDCC gating is not exclusively controlled physically by the voltage sensor and the pore-lining helices but rather by a complex, conserved, and exact physical organization of those elements with the intracellular domains like the I-II linker/β complex. Thus, intracellular elements impinge directly on gating in a manner partially akin to the MthK, KirBac, and Girk channels, gated by ligand binding of intracellular domains (Jiang et al., 2002a; Kuo et al., 2003; Nishida and MacKinnon, 2002).
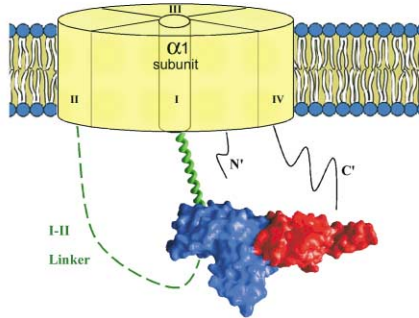
How might these intracellular elements like the I-II linker/β complex impinge on gating? We envisage three aspects. First, the AID-β complex structure demonstrates that the AID and β almost seamlessly fuse into a united surface. The resulting electrostatic potential produced shows that β domain II has a patch of negative potential (Figure 6B), coincident and contiguous to the locale of AID binding. This patch will react to changes in the electrostatic potential of the surrounding environment as a result of membrane depolarization and the channel opening with its flux of Ca^{2+} ions diffusing from the channel mouth. Hence, the bound β reconfigures the electrostatics of the intracellular side of the channel. Second, β orders a part of the channel physically connected to its gate, essentially changing its shape, length, and mechanical properties, such as rigidity. Third, through β binding, the gate is now connected to a linker with much greater mass and depending on isoform constrained in its movement by its own independent attachment to the membrane.

Of the known modulatory effects of β, one common denominator is that β seems to shift the equilibrium toward the open channel state, i.e., activation. All three aspects of the I-II linker/β just described should facilitate this effect. Upon depolarization, the I-II linker/β negative patch may move in reaction to the changing electrostatic

(B) Close-up view of AID/β interactions with relevant side chains labeled. Dashed lines indicate hydrogen bonds. Helices 4.1 and 4.2 comprise the lid subdomain.
(C) Table of AID mutations abstracted from the literature (Berrou et al., 2002; De Waard et al., 1996; Witcher et al., 1995). Binding to β is the effect charted on a scale of no binding (-) to wt binding (4 stars).
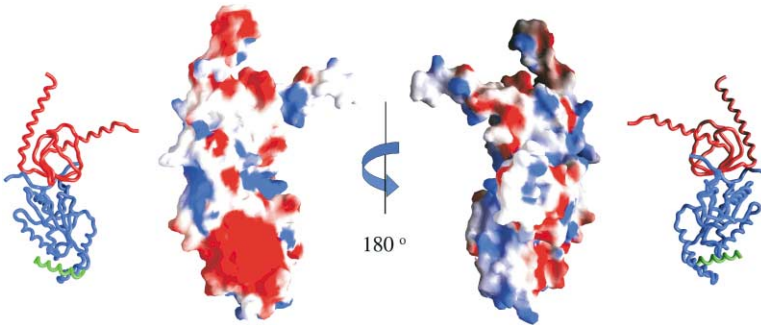
A

B

potential of α1 (Cens et al., 1998), supplementing the radial torque on S6 from the voltage sensor. The presumed helical conformation will lend the requisite rigidity for any movements of the AID-β particle to be communicated to the gate. Also, the additional mass weighing on membrane domain I may destabilize the closed conformation of its S6. Thus, β's action on the channel state is best categorized as allosteric modulation.

Regarding channel inactivation and its kinetics, our structural model fits well with current models that propose a hinged lid mechanism (Stotz et al., 2004). Here, the AID/β surface serves as the lid, the channel opens, and Ca^{2+} accumulates at the mouth and attracts the lid by Coulombic forces and in coordination with Ca^{2+}-dependent inactivation determinants of the α1 C terminus (Cens et al., 1999). Subsequently, residues in the AID that are solvent exposed (i.e., those not involved in binding β and other residues of the linker) find their receptor site possibly in the channel mouth, thereby blocking ion flow and inactivating the channel. According to this inactivation mechanism, the hinge that enables the lid to swivel may be located at the link between S6 and the I-II linker (i.e., the conserved glycine sequence at its start). Another prediction of this model will be the slowing of inactivation if β's movement is constrained through its N terminus since the "lid" would then not be able to move as easily toward the channel mouth. This notion then explains the slow inactivation of β2a whose N terminus is anchored in the membrane

by palmitoylation. When the palmitoylation site is mutated, inactivation parameters resemble that of the other isoforms and splice variants (Olcese et al., 1994; Restituito et al., 2000; Stephens et al., 2000).

The structure of β determined represents only part of the molecule. For β3, the functional core represents about 70% of the molecule while it is less for the other isoforms. Many studies have demonstrated functions encoded by regions outside of the core, such as inactivation, influenced by the N terminus or the linker between β domains I and II (Walker and De Waard, 1998). Likewise, the C terminus, whose size and sequence varies dramatically between isoforms, has been shown to be important for binding other sites on the α1 subunit (Walker et al., 1999). The functional core architecture, therefore, maintains the central functions of the molecule. At the same time, extraneous polypeptide regions elaborate functional specificity. Furthermore, functional specificity may be tuned not only by isoform but also by splicing alterations (Dolphin, 2003a). These splicing permutations fall outside the core architecture.

In conclusion, the data presented here have novel implications for VDCC β function that extend outside the context of the VDCC itself. Specifically, the molecular architecture of the β functional core argues strongly that this protein has evolved to maximize protein-protein interactions with other partners. Recent examples of novel proteins that associate with β are the members of the small G protein subfamily, Gem, Rad, and Rem

(Beguin et al., 2001; Finlin et al., 2003; Ward et al., 2004), and HP1γ, involved in gene silencing (Hibino et al., 2003). Taken together, these findings strongly suggest that β serves as a nexus of the signaling pathways tied to calcium and hence open up new directions of investigation toward their full elucidation.

Experimental Procedures

Expression and Purification

Selenomethionine-substituted VDCC β functional core was prepared and crystallized for multiwavelength anomalous diffraction (MAD). Protein was produced in *E. coli* BL21 (DE3) as described (Opatowsky et al., 2004), by inhibition of the methionine pathway (Van Duyne et al., 1993). An overnight starter culture was grown from a single transformed colony in 10% LB medium. LB media was removed prior to the introduction of 2 l of New Minimal Media (Budisa et al., 1995), fortified with Kao and Michayluk vitamin solution (Sigma), 100 μg/ml ampicillin, and 34 μg/ml chloramphenicol. Cells were grown at 37°C to $OD_{600} = 0.3$, whereupon the temperature was lowered to 16°C. Lysine, phenylalanine, and threonine (100 mg/l), isoleucine, leucine, and valine (50 mg/l), and DL-selenomethionine (50 mg/l) were added 45 min before induction ($A_{600} = 0.6$). Expression was induced with 200 μM IPTG over a 14 hr period. Purification of the SeMet protein was similar to that of the native protein (Opatowsky et al., 2004), except that 5 mM β-ME was added to all solutions to prevent oxidation. The efficiency of SeMet incorporation was confirmed by mass spectrometry.

Crystallization and Structure Determination

SeMet protein crystals were grown at 19°C by hanging drop vapor diffusion with conditions near those of native protein (Opatowsky et al., 2004). Equal volumes (1–2 μl) of diluted frozen stock protein (6–12 mg/ml) were mixed with reservoir solution containing 1%–4% PEG 20K, 0.1 M Bicine (pH 9), 1%–3% MPD, and 5 mM β-mercaptoethanol. Orthorhombic crystals were allowed to grow for no longer than 20 hr, then cryoprotected by sequential dilutions with mother liquor added with 35% glycerol. The crystals were mounted in cryoloops and flash frozen with liquid N_2.

For cocrystallization of VDCC β functional core and purified AID peptide, equal volumes of equimolar (1–2 μl; 300 μM) protein and peptide were mixed and equilibrated for 30 min. This solution was screened by hanging drops and gave cocrystals at about the same conditions as described above. Cocrystals have the same space group symmetry as protein crystals with similar unit cell dimensions.

Diffraction data for the SeMet protein crystals and the cocrystals were measured at the ESRF, under standard cryogenic conditions, and processed with HKL software package (Otwinowski and Minor, 1997). A three-wavelength MAD experiment was performed on a single SeMet protein crystal (Tables 1 and 2). The anomalous absorption peak, followed by its inflection point and a remote with some anomalous signal, were chosen for the wavelengths. Scaled data sets for each wavelength were then rescaled by local scaling and 6 selenium sites located using SOLVE (Terwilliger, 2003). A clear heavy atom solution was obtained and heavy atom parameters refined to produce experimental phases, using SOLVE. These phases were then used for density modification by RESOLVE (Terwilliger, 2003) or SOLOMON (Abrahams and Leslie, 1996), whose outputs gave two complementary 2.9 Å electron density maps of high quality. A model of β was built with O (Jones et al., 1991) and refined with CNS (Brünger et al., 1998). At that point, we refined the model against a nonisomorphous 2.3 Å data set using CNS, REFMAC5 (Murshudov et al., 1997), and ARP (Morris et al., 2003) with rounds of model rebuilding.

The β/AID peptide cocrystal structure was determined by molecular replacement. Initially, we used a 3 Å data set measured on our home source. Despite the similarity in crystal forms between the β crystals and the cocrystals, rigid body refinement was not sufficient to obtain electron density maps showing the peptide. After molecular replacement (MR) with CNS, using the 2.3 Å refined β model, clear and unmistakable density was found for the bound peptide. MR was required due to a shift of β by several angstroms along

one axis. The peptide model was built including changes in β and refined against a 2.2 Å data set collected subsequently. Rounds of model building and refinement were performed as above. The current models have good stereochemistry (Laskowski et al., 1993). Both of these crystals utilized protein that bears a mutation in domain I that does not affect function (Opatowsky et al., 2003).

Diffraction data were collected on an alternative crystal form described previously (Opatowsky et al., 2004). This crystal form diffracts to about 3.5 Å and could be obtained using both wt and mutant protein, as well as truncated linker core and linkerless core proteins. Electron density maps and models of the truncated linker core and linkerless tetragonal crystals were obtained by MR with MolRep (Vagin and Teplyakov, 2000), using the 2.3 Å β model. No gross changes in structure were noted between the wt and mutant protein nor between truncated linker core and linkerless core proteins.

In Vitro Binding Assays

Full-length VDCC β2a was mutated by the QuikChange (Stratagene) method. The altered sequence was confirmed by DNA sequencing. Expression, purification, and fluorescence polarization measurements of the mutant proteins were as described (Opatowsky et al., 2003).

CD Spectroscopy

CD measurements were performed with an Aviv CD spectrometer model 202. Spectra were measured over the range of 260–180 nm at a scan rate of 1 nm/s. For all measurements, a cell with 1 mm path length was used. The raw data were corrected by subtracting the contribution of the buffer to the CD signal. Data were smoothed and converted to molar ellipticity units. Concentration of peptide was obtained using its predicted extinction coefficient at 280 nm.

Molecular Graphics

Figures 1, 3A, 3B, and 4A were made with Bobscript (Esnouf, 1999) and Raster3D (Merritt and Bacon, 1997). Figures 3C and 4B were prepared with Molscript (Kraulis, 1991) and Raster3D. Figure 6 was prepared with GRASP (Nicholls et al., 1991).

References

Abrahams, J.P., and Leslie, A.G.W. (1996). Methods used in the structure determination of bovine mitochondrial F-1 ATPase. Acta Crystallogr. D *52*, 30–42.

Andersen, C.A., Palmer, A.G., Brunak, S., and Rost, B. (2002). Continuum secondary structure captures protein flexibility. Structure *10*, 175–184.

Ball, S.L., Powers, P.A., Shin, H.S., Morgans, C.W., Peachey, N.S., and Gregg, R.G. (2002). Role of the beta(2) subunit of voltage-dependent calcium channels in the retinal outer plexiform layer. Invest. Ophthalmol. Vis. Sci. *43*, 1595–1603.

Beguin, P., Nagashima, K., Gonoi, T., Shibasaki, T., Takahashi, K., Kashima, Y., Ozaki, N., Geering, K., Iwanaga, T., and Seino, S. (2001). Regulation of Ca^{2+} channel expression at the cell surface by the small G-protein kir/Gem. Nature *411*, 701–706.

Berrou, L., Klein, H., Bernatchez, G., and Parent, L. (2002). A specific tryptophan in the I–II linker is a key determinant of beta-subunit binding and modulation in Ca(V)2.3 calcium channels. Biophys. J. 83, 1429–1442.

Bichet, D., Cornet, V., Geib, S., Carlier, E., Volsen, S., Hoshi, T., Mori, Y., and De Waard, M. (2000a). The I–II loop of the Ca^{2+} channel alpha1 subunit contains an endoplasmic reticulum retention signal antagonized by the beta subunit. Neuron 25, 177–190.

Bichet, D., Lecomte, C., Sabatier, J.M., Felix, R., and De Waard, M. (2000b). Reversibility of the Ca(2+) channel alpha(1)-beta subunit interaction. Biochem. Biophys. Res. Commun. 277, 729–735.

Bohm, G., Muhr, R., and Jaenicke, R. (1992). Quantitative analysis of protein far UV circular dichroism spectra by neural networks. Protein Eng. 5, 191–195.

Brünger, A.T., Adams, P.D., Clore, G.M., DeLano, W.L., Gros, P., Grosse-Kunstleve, R.W., Jiang, J.-S., Kuszewki, J., Nilges, M., Pannu, N.S., et al. (1998). Crystallography & NMR system: a new software suite for macromolecular structure determination. Acta Crystallogr. D 54, 905–921.

Budisa, N., Steipe, B., Demange, P., Eckerskorn, C., Kellermann, J., and Huber, R. (1995). High-level biosynthetic substitution of methionine in proteins by its analogs 2-aminohexanoic acid, selenomethionine, telluromethionine and ethionine in Escherichia coli. Eur. J. Biochem. 230, 788–796.

Budnik, V., Koh, Y.H., Guan, B., Hartmann, B., Hough, C., Woods, D., and Gorczyca, M. (1996). Regulation of synapse structure and function by the Drosophila tumor suppressor gene dlg. Neuron 17, 627–640.

Canti, C., Page, K.M., Stephens, G.J., and Dolphin, A.C. (1999). Identification of residues in the N terminus of alpha1B critical for inhibition of the voltage-dependent calcium channel by Gbeta gamma. J. Neurosci. 19, 6855–6864.

Canti, C., Davies, A., Berrow, N.S., Butcher, A.J., Page, K.M., and Dolphin, A.C. (2001). Evidence for two concentration-dependent processes for beta-subunit effects on alpha1B calcium channels. Biophys. J. 81, 1439–1451.

Catterall, W.A. (1996). Molecular properties of sodium and calcium channels. J. Bioenerg. Biomembr. 28, 219–230.

Cens, T., Dalle, C., and Charnet, P. (1998). Expression of beta subunit modulates surface potential sensing by calcium channels. Pflugers Arch. 435, 865–867.

Cens, T., Restituito, S., Galas, S., and Charnet, P. (1999). Voltage and calcium use the same molecular determinants to inactivate calcium channels. J. Biol. Chem. 274, 5483–5490.

Chien, A.J., Zhao, X., Shirokov, R.E., Puri, T.S., Chang, C.F., Sun, D., Rios, E., and Hosey, M.M. (1995). Roles of a membrane-localized beta subunit in the formation and targeting of functional L-type Ca^{2+} channels. J. Biol. Chem. 270, 30036–30044.

Chien, A.J., Gao, T., Perez-Reyes, E., and Hosey, M.M. (1998). Membrane targeting of L-type calcium channels. Role of palmitoylation in the subcellular localization of the beta2a subunit. J. Biol. Chem. 273, 23590–23597.

Cornet, V., Bichet, D., Sandoz, G., Marty, I., Brocard, J., Bourinet, E., Mori, Y., Villaz, M., and De Waard, M. (2002). Multiple determinants in voltage-dependent P/Q calcium channels control their retention in the endoplasmic reticulum. Eur. J. Neurosci. 16, 883–895.

De Waard, M., Pragnell, M., and Campbell, K.P. (1994). Ca^{2+} channel regulation by a conserved beta subunit domain. Neuron 13, 495–503.

De Waard, M., Scott, V.E., Pragnell, M., and Campbell, K.P. (1996). Identification of critical amino acids involved in alpha1-beta interaction in voltage-dependent Ca^{2+} channels. FEBS Lett. 380, 272–276.

Dimitratos, S.D., Woods, D.F., Stathakis, D.G., and Bryant, P.J. (1999). Signaling pathways are focused at specialized regions of the plasma membrane by scaffolding proteins of the MAGUK family. Bioessays 21, 912–921.

Dolphin, A.C. (2003a). β subunits of voltage-gated calcium channels. J. Bioenerg. Biomembr. 35, 599–620.

Dolphin, A.C. (2003b). G protein modulation of voltage-gated calcium channels. Pharmacol. Rev. 55, 607–627.

Esnouf, R.M. (1999). Further additions to MolScript version 1.4, including reading and contouring of electron-density maps. Acta Crystallogr. D 55, 938–940.

Finlin, B.S., Crump, S.M., Satin, J., and Andres, D.A. (2003). Regulation of voltage-gated calcium channel activity by the Rem and Rad GTPases. Proc. Natl. Acad. Sci. USA 100, 14469–14474.

Geib, S., Sandoz, G., Mabrouk, K., Matavel, A., Marchot, P., Hoshi, T., Villaz, M., Ronjat, M., Miquelis, R., Leveque, C., and de Waard, M. (2002). Use of a purified and functional recombinant calcium-channel beta4 subunit in surface-plasmon resonance studies. Biochem. J. 364, 285–292.

Hanada, T., Lin, L., Tibaldi, E.V., Reinherz, E.L., and Chishti, A.H. (2000). GAKIN, a novel kinesin-like protein associates with the human homologue of the Drosophila discs large tumor suppressor in T lymphocytes. J. Biol. Chem. 275, 28774–28784.

Hanlon, M.R., Berrow, N.S., Dolphin, A.C., and Wallace, B.A. (1999). Modelling of a voltage-dependent Ca^{2+} channel beta subunit as a basis for understanding its functional properties. FEBS Lett. 445, 366–370.

Herlitze, S., Xie, M., Han, J., Hummer, A., Melnik-Martinez, K.V., Moreno, R.L., and Mark, M.D. (2003). Targeting mechanisms of high voltage-activated Ca^{2+} channels. J. Bioenerg. Biomembr. 35, 621–637.

Hibino, H., Pironkova, R., Onwumere, O., Rousset, M., Charnet, P., Hudspeth, A.J., and Lesage, F. (2003). Direct interaction with a nuclear protein and regulation of gene silencing by a variant of the Ca^{2+}-channel beta 4 subunit. Proc. Natl. Acad. Sci. USA 100, 307–312.

Jiang, Y., Lee, A., Chen, J., Cadene, M., Chait, B.T., and MacKinnon, R. (2002a). Crystal structure and mechanism of a calcium-gated potassium channel. Nature 417, 515–522.

Jiang, Y., Lee, A., Chen, J., Cadene, M., Chait, B.T., and MacKinnon, R. (2002b). The open pore conformation of potassium channels. Nature 417, 523–526.

Jones, S.W. (1998). Overview of voltage-dependent calcium channels. J. Bioenerg. Biomembr. 30, 299–312.

Jones, T.A., Zou, J.-Y., Cowan, S.W., and Kjeldgaard, M. (1991). Improved methods for building protein models in electron density maps and the location of errors in these models. Acta Crystallogr. A 47, 110–119.

Kim, E., Naisbitt, S., Hsueh, Y.P., Rao, A., Rothschild, A., Craig, A.M., and Sheng, M. (1997). GKAP, a novel synaptic protein that interacts with the guanylate kinase-like domain of the PSD-95/SAP90 family of channel clustering molecules. J. Cell Biol. 136, 669–678.

Kraulis, P.J. (1991). Molscript—a program to produce both detailed and schematic plots of protein structures. J. Appl. Crystallogr. 24, 946–950.

Kuo, A., Gulbis, J.M., Antcliff, J.F., Rahman, T., Lowe, E.D., Zimmer, J., Cuthbertson, J., Ashcroft, F.M., Ezaki, T., and Doyle, D.A. (2003). Crystal structure of the potassium channel KirBac1.1 in the closed state. Science 300, 1922–1926.

Laskowski, R.A., Macarthur, M.W., Moss, D.S., and Thornton, J.M. (1993). Procheck—a program to check the stereochemical quality of protein structures. J. Appl. Crystallogr. 26, 283–291.

Leipe, D.D., Koonin, E.V., and Aravind, L. (2003). Evolution and classification of P-loop kinases and related proteins. J. Mol. Biol. 333, 781–815.

Lo Conte, L., Chothia, C., and Janin, J. (1999). The atomic structure of protein-protein recognition sites. J. Mol. Biol. 285, 2177–2198.

Luo, P., and Baldwin, R.L. (1997). Mechanism of helix induction by trifluoroethanol: a framework for extrapolating the helix-forming properties of peptides from trifluoroethanol/water mixtures back to water. Biochemistry 36, 8413–8421.

Marquart, A.F.V. (1997). Alpha-1-beta interaction in voltage-gated cardiac L-type calcium channels. FEBS Lett. 407, 137–140.

Mathew, D., Gramates, L.S., Packard, M., Thomas, U., Bilder, D., Perrimon, N., Gorczyca, M., and Budnik, V. (2002). Recruitment of scribble to the synaptic scaffolding complex requires GUK-holder, a novel DLG binding protein. Curr. Biol. 12, 531–539.

McGee, A.W., Dakoji, S.R., Olsen, O., Bredt, D.S., Lim, W.A., and Prehoda, K.E. (2001). Structure of the SH3-guanylate kinase module from PSD-95 suggests a mechanism for regulated assembly of MAGUK scaffolding proteins. Mol. Cell 8, 1291–1301.

Meinhart, A., Alonso, J.C., Strater, N., and Saenger, W. (2003). Crystal structure of the plasmid maintenance system epsilon/zeta: functional mechanism of toxin zeta and inactivation by epsilon 2 zeta 2 complex formation. Proc. Natl. Acad. Sci. USA 100, 1661–1666.

Merritt, E.A., and Bacon, D.J. (1997). Raster3D: photorealistic molecular graphics. In Methods in Enzymology, Volume 277, C.W. Carter, Jr., and R.M. Sweet, eds. (New York: Academic Press), pp. 505–524.

Morris, R.J., Perrakis, A., and Lamzin, V.S. (2003). ARP/wARP and automatic interpretation of protein electron density maps. Methods Enzymol. 374, 229–244.

Murata, K., Odahara, N., Kuniyasu, A., Sato, Y., Nakayama, H., and Nagayama, K. (2001). Asymmetric arrangement of auxiliary subunits of skeletal muscle voltage-gated l-type Ca(2+) channel. Biochem. Biophys. Res. Commun. 282, 284–291.

Murshudov, G.N., Vagin, A.A., and Dodson, E.J. (1997). Refinement of macromolecular structures by the maximum-likelihood method. Acta Crystallogr. D 53, 240–255.

Nicholls, A., Sharp, K.A., and Honig, B. (1991). Protein folding and association: insights from the interfacial and thermodynamic properties of hydrocarbons. Proteins 11, 281–296.

Nishida, M., and MacKinnon, R. (2002). Structural basis of inward rectification: cytoplasmic pore of the G protein-gated inward rectifier GIRK1 at 1.8 Å resolution. Cell 111, 957–965.

Olcese, R., Qin, N., Schneider, T., Neely, A., Wei, X., Stefani, E., and Birnbaumer, L. (1994). The amino terminus of a calcium channel beta subunit sets rates of channel inactivation independently of the subunit's effect on activation. Neuron 13, 1433–1438.

Opatowsky, Y., Chomsky-Hecht, O., Kang, M.G., Campbell, K.P., and Hirsch, J.A. (2003). The voltage-dependent calcium channel beta subunit contains two stable interacting domains. J. Biol. Chem. 278, 52323–52332.

Opatowsky, Y., Chomsky-Hecht, O., and Hirsch, J.A. (2004). Expression, purification, and crystallization of a functional core of the voltage dependent calcium channel β subunit. Acta Crystallogr. D., in press.

Otwinowski, Z., and Minor, W. (1997). Processing of X-ray diffraction data collected in oscillation mode. In Methods in Enzymology, Volume 276, C.W. Carter, Jr., and R.M. Sweet, eds. (New York: Academic Press), pp. 307–326.

Pace, C.N., and Scholtz, J.M. (1998). A helix propensity scale based on experimental studies of peptides and proteins. Biophys. J. 75, 422–427.

Pragnell, M., De Waard, M., Mori, Y., Tanabe, T., Snutch, T.P., and Campbell, K.P. (1994). Calcium channel beta-subunit binds to a conserved motif in the I–II cytoplasmic linker of the alpha 1-subunit. Nature 368, 67–70.

Restituito, S., Cens, T., Barrere, C., Geib, S., Galas, S., De Waard, M., and Charnet, P. (2000). The [beta]2a subunit is a molecular groom for the Ca²⁺ channel inactivation gate. J. Neurosci. 20, 9046–9052.

Restituito, S., Cens, T., Rousset, M., and Charnet, P. (2001). Ca(2+) channel inactivation heterogeneity reveals physiological unbinding of auxiliary beta subunits. Biophys. J. 81, 89–96.

Schreiber, G. (2002). Kinetic studies of protein-protein interactions. Curr. Opin. Struct. Biol. 12, 41–47.

Sekulic, N., Shuvalova, L., Spangenberg, O., Konrad, M., and Lavie, A. (2002). Structural characterization of the closed conformation of mouse guanylate kinase. J. Biol. Chem. 277, 30236–30243.

Serysheva, I.I., Ludtke, S.J., Baker, M.R., Chiu, W., and Hamilton, S.L. (2002). Structure of the voltage-gated L-type Ca²⁺ channel by electron cryomicroscopy. Proc. Natl. Acad. Sci. USA 99, 10370–10375.

Shatsky, M., Nussinov, R., and Wolfson, H.J. (2002). Flexible protein alignment and hinge detection. Proteins 48, 242–256.

Stehle, T., and Schulz, G.E. (1992). Refined structure of the complex between guanylate kinase and its substrate GMP at 2.0 Å resolution. J. Mol. Biol. 224, 1127–1141.

Stephens, G.J., Page, K.M., Bogdanov, Y., and Dolphin, A.C. (2000). The alpha1B Ca²⁺ channel amino terminus contributes determinants for beta subunit-mediated voltage-dependent inactivation properties. J. Physiol. 525, 377–390.

Stotz, S.C., Jarvis, S.E., and Zamponi, G.W. (2004). Functional roles of cytoplasmic loops and pore lining transmembrane helices in the voltage-dependent inactivation of HVA calcium channels. J. Physiol. 554, 263–273.

Takeuchi, M., Hata, Y., Hirao, K., Toyoda, A., Irie, M., and Takai, Y. (1997). SAPAPs. A family of PSD-95/SAP90-associated proteins localized at postsynaptic density. J. Biol. Chem. 272, 11943–11951.

Tanabe, T., Takeshima, H., Mikami, A., Flockerzi, V., Takahashi, H., Kangawa, K., Kojima, M., Matsuo, H., Hirose, T., and Numa, S. (1987). Primary structure of the receptor for calcium channel blockers from skeletal muscle. Nature 328, 313–318.

Tareilus, E., Roux, M., Qin, N., Olcese, R., Zhou, J., Stefani, E., and Birnbaumer, L. (1997). A Xenopus oocyte beta subunit: evidence for a role in the assembly/expression of voltage-gated calcium channels that is separate from its role as a regulatory subunit. Proc. Natl. Acad. Sci. USA 94, 1703–1708.

Tavares, G.A., Panepucci, E.H., and Brunger, A.T. (2001). Structural characterization of the intramolecular interaction between the SH3 and guanylate kinase domains of PSD-95. Mol. Cell 8, 1313–1325.

Terwilliger, T.C. (2003). SOLVE and RESOLVE: automated structure solution and density modification. Methods Enzymol. 374, 22–37.

Vagin, A., and Teplyakov, A. (2000). An approach to multi-copy search in molecular replacement. Acta Crystallogr. D Biol. Crystallogr. 56, 1622–1624.

Van Duyne, G.D., Standaert, R.F., Karplus, P.A., Schreiber, S.L., and Clardy, J. (1993). Atomic structures of the human immunophilin FKBP-12 complexes with FK506 and rapamycin. J. Mol. Biol. 229, 105–124.

Walker, D., and De Waard, M. (1998). Subunit interaction sites in voltage-dependent Ca²⁺ channels: role in channel function. Trends Neurosci. 21, 148–154.

Walker, D., Bichet, D., Campbell, K.P., and Dewaard, M. (1998). A beta4 isoform-specific interaction site in the carboxyl-terminal region of the voltage-dependent Ca²⁺ channel alpha(1a) subunit. J. Biol. Chem. 273, 2361–2367.

Walker, D., Bichet, D., Geib, S., Mori, E., Cornet, V., Snutch, T.P., Mori, Y., and De Waard, M. (1999). A new beta subtype-specific interaction in alpha1A subunit controls P/Q- type Ca²⁺ channel activation. J. Biol. Chem. 274, 12383–12390.

Wang, M.C., Collins, R.F., Ford, R.C., Berrow, N.S., Dolphin, A.C., and Kitmitto, A. (2003). The three-dimensional structure of the cardiac L-type voltage-gated calcium channel: comparison with the skeletal muscle form reveals a common architectural motif. J. Biol. Chem. 279, 7159–7168.

Ward, Y., Spinelli, B., Quon, M.J., Chen, H., Ikeda, S.R., and Kelly, K. (2004). Phosphorylation of critical serine residues in gem separates cytoskeletal reorganization from down-regulation of calcium channel activity. Mol. Cell. Biol. 24, 651–661.

Witcher, D.R., De Waard, M., Liu, H., Pragnell, M., and Campbell, K.P. (1995). Association of native Ca²⁺ channel beta subunits with the alpha 1 subunit interaction domain. J. Biol. Chem. 270, 18088–18093.

Wolf, M., Eberhart, A., Glossmann, H., Striessnig, J., and Grigorieff, N. (2003). Visualization of the domain structure of an L-type Ca²⁺ channel using electron cryo-microscopy. J. Mol. Biol. 332, 171–182.

Wu, X., Knudsen, B., Feller, S.M., Zheng, J., Sali, A., Cowburn, D., Hanafusa, H., and Kuriyan, J. (1995). Structural basis for the specific interaction of lysine-containing proline-rich peptides with the N-terminal SH3 domain of c-Crk. Structure 3, 215–226.

Yang, A.S., and Honig, B. (1995). Free energy determinants of secondary structure formation: I. alpha-helices. J. Mol. Biol. 252, 351–365.

Accession Numbers

The Protein Data Bank accession codes for β and the AID/β complexes are 1T3S and 1T3L, respectively.